Structural properties of glasses in the series $(SrO)_x(V_2O_5)_{1-x}$, $(SrO)_{0.5-y}(B_2O_3)_y(V_2O_5)_{0.5}$, and $(SrO)_{0.2}(B_2O_3)_z(V_2O_5)_{0.8-z}$

G. D. Khattak and N. Tabet
Department of Physics, King Fahd University of Petroleum and Minerals, Dhahran 31261, Saudi Arabia

L. E. Wenger
Department of Physics, The University of Alabama at Birmingham, Birmingham, Alabama 35294-1170, USA
(Received 27 April 2005; published 9 September 2005)

In order to further elucidate the local structure of vanadate glasses, x-ray photoelectron spectroscopy (XPS) and magnetization studies are reported on a series of SrO-vanadate and SrO-borovanadate glasses: $[(SrO)_x(V_2O_5)_{1-x}]$, $[(SrO)_{0.5-y}(B_2O_3)_y(V_2O_5)_{0.5}]$, and $[(SrO)_{0.2}(B_2O_3)_z(V_2O_5)_{0.8-z}]$. From the analysis of the XPS spectra for the Sr 3*p*, B 1*s*, V 2*p*, and O 1*s* core levels, several distinct concentration regimes are identified in terms of various structural units being present. Metavanadate chainlike structures of SrV_2O_6 and individual VO_4 units occur in vanadate glasses with low SrO content $x \leqslant 0.2$ with VO_5 polyhedra also appearing at higher SrO content. The SrV_2O_6 and VO_n polyhedra predominate in the low B_2O_3 containing SrO-borovanadate glasses as the B substitutes into the V sites of the various VO_n polyhedra and only when the B_2O_3 concentration exceeds the SrO content do BO_n structures appear. This qualitative picture of three distinct structural groupings for the Sr-vanadate and Sr-borovanadate glasses is consistent with the proposed glass structure based on previous IR and extended x-ray absorption fine structure (EXAFS) studies on these types of vanadate glasses.

DOI: 10.1103/PhysRevB.72.104203 PACS number(s): 61.14.Qp, 61.43.Fs, 75.20.−g

I. INTRODUCTION

Studies of transition-metal (TM) oxide glasses continue to be of interest because of their semiconducting properties and the corresponding potential applicability to electronic devices.[1–4] The semiconducting behavior in these glasses arises from an unpaired $3d^1$ electron hopping between TM ions[5,6] when the TM ions exist in two or more valence states, e.g., from an electron hopping from a V^{4+} site to a V^{5+} site. Because the unpaired electron induces a polarization around the TM ion, conduction can be described in terms of a model based on polarons. However, a more detailed modeling of the conduction process is limited because of numerous material factors, including the type and concentration of the TM ion, the number of valence states associated with the TM ion, the glass preparation conditions, and the microstructures within the glass matrix. Thus, information on the structure of a glass is imperative for further elucidating an understanding of the glass properties.

Although the existence of binary and ternary V_2O_5 glasses is well established and various properties have been studied,[7–29] the structure of vanadate glasses remains a subject of interest because there is no clear picture as to the exact nature of the oxygen polyhedra surrounding the vanadium atoms or of the role played by the other glass components. Even in the case of pure V_2O_5 glass it has been reported[30,31] that V^{5+} ions exhibit both four and fivefold coordination states, depending on the sample preparation conditions. Moreover, the structure of the vanadate glasses can be related to the nature of the network formers as well as on the network modifiers. For example, previous structural studies on alkaline earth vanadate glasses by NMR and IR spectroscopy techniques[15–17] suggest that the local structure of these glasses is basically the same, irrespective of the alkaline-earth metal, and consists mainly of corner-sharing VO_4 tetrahedra. On the other hand, a neutron-diffraction investigation on barium and lead vanadate glasses[13,14] indicates that the vanadate network is composed of distorted, interconnected VO_5 trigonal bipyramids and/or tetragonal pyramids. Other studies of the structural properties have reported that V_2O_5 acts as a network former[18–21] and consists of unaffected VO_5 groups as in vitreous V_2O_5 and affected VO_5 groups with alkaline-earth ions. This is in contrast to the vanadate glasses formed by conventional network formers in which only unaffected VO_5 groups are present.[11]

X-ray photoelectron spectroscopy (XPS) is an important and powerful technique for investigating the electronic structure and chemical bonding in solids as well as in describing the local structure.[32–35] When a specimen is irradiated with a beam of x-rays, photoelectrons are ejected from its atoms with kinetic energies E_k. From the conservation of energy, the binding energy E_B of the emitted photoelectrons is essentially given by $E_B = h\upsilon - E_k - W - C$, where $h\upsilon$ is the energy of the incident x-ray radiation, W is the work function of the spectrometer, and C is an energy shift induced by surface charging effects. The binding energy of the emitted electron and, correspondingly, the measured kinetic energy of the photoelectron will be determined by the atomic orbital in question, which itself is characteristic of the material depending on the local chemical or structural configuration. This effect is termed the "chemical shift," which is on the order of 0.5–5 eV as compared to the 100–1000 eV energy spectrum that can be detected. XPS has also been shown to be a useful quantitative probe of the short-range structure in the oxide glasses.[36] In particular, the O 1*s* spectrum can be resolved into separate contributions from bridging and non-

TABLE I. Nominal and actual molar composition of Sr-vanadate [I] and Sr-borovanadate [II and III] glasses. The uncertainty in the ICP analysis of the molar fraction is ±5%.

Series	Nominal	SrO	B_2O_3	V_2O_5
I	$x=0.2$	0.208		0.792
$(SrO)_x(V_2O_5)_{1-x}$	$x=0.3$	0.308		0.692
	$x=0.4$	0.409		0.591
	$x=0.5$	0.511		0.488
II	$y=0.0$	0.511		0.488
$(SrO)_{0.5-y}(B_2O_3)_y(V_2O_5)_{0.5}$	$y=0.1$	0.415	0.087	0.498
	$y=0.2$	0.299	0.218	0.483
	$y=0.3$	0.192	0.322	0.486
	$y=0.4$	0.112	0.347	0.539
III	$z=0.0$	0.208		0.792
$(SrO)_{0.2}(B_2O_3)_z(V_2O_5)_{0.8-z}$	$z=0.1$	0.209	0.091	0.707
	$z=0.2$	0.209	0.178	0.613
	$z=0.3$	0.194	0.313	0.493
	$z=0.4$	0.220	0.346	0.434

bridging oxygen, which result from different structural units of the oxygen atoms in these oxide glasses. Furthermore, the valence state of the TM ions in the glass structure can be investigated and their relative concentrations can be determined.[36] To provide an independent determination of the ratio of the different valence states of V present in these glasses, magnetization measurements combined with inductively coupled plasma (ICP) spectroscopy were undertaken. Thus, the present XPS study combined with magnetization measurements on a series of Sr-vanadate and Sr-borovanadate glasses has permitted the identification of the local glass structure in terms of different vanadate structural units for various concentration regimes that are consistent with the proposed structures based on previous IR and extended x-ray-absorption fine structure (EXAFS) studies.[11,26,27]

II. EXPERIMENTAL METHODS

A. Sample preparation

The three series of glasses investigated in this paper were prepared by melting dry mixtures of reagent grade V_2O_5, B_2O_3, and SrO in alumina crucibles with nominal compositions $[(SrO)_x(V_2O_5)_{1-x}]$, $0.2 \leqslant x \leqslant 0.5$, $[(SrO)_{0.5-y}(B_2O_3)_y(V_2O_5)_{0.5}]$, $0.0 \leqslant y \leqslant 0.4$, and $[(SrO)_{0.2}(B_2O_3)_z(V_2O_5)_{0.8-z}]$ with $0.0 \leqslant z \leqslant 0.4$. Because the oxidation and reduction reactions in a glass melt are known to depend on the size of the melt, on the sample geometry, on whether the melt is static or stirred, on thermal history, and on quenching rate, all glass samples were prepared under similar conditions to standardize these factors. Approximately 30 g of chemicals were thoroughly mixed to obtain a homogenized mixture for each V_2O_5 concentration. The crucible containing the batch mixture was then transferred to an electrically heated melting furnace maintained at 1000–1100 °C, depending on the composition of the sample. The melt was left for about 1 h under atmospheric conditions in the furnace during which the melt was occasionally stirred with an alumina rod. The homogenized melt was then cast onto a stainless-steel plate mold to form glass buttons and glass rods of ~5 mm diam for XPS measurements. After casting, the specimens were annealed at 200 °C for 2 h. X-ray-powder-diffraction patterns indicated that the glasses formed were completely amorphous. After preparation, the samples were stored in a vacuum desiccator to minimize any further oxidation of the glass samples. The actual compositions of the glasses were determined by inductively coupled plasma (ICP) spectroscopy and are listed in Table I. Although the inclusion of alumina from the crucibles used in the melting of the glass mixtures is a possible source of impurities,[38] no signals for aluminum were detected in both the XPS and ICP studies of these glasses.

B. Measurement techniques

XPS photoelectron spectra of the V $2p$, Sr $3p$, B $1s$, and O $1s$ core levels were collected on a VG scientific ESCALAB MKII spectrometer equipped with dual aluminum-magnesium anode x-ray gun and a 150 mm concentric hemispherical analyzer using Al $K\alpha$ ($h\nu$ = 1486.6 eV) radiation from an anode operated at 130 W. The electron analyzer was set at pass energy of 20 eV with the energy scale of the spectrometer calibrated using the core level of Cu $2p_{3/2}$ (932.67 eV), Cu $3p_{3/2}$ (74.9 eV), and Au $4f_{7/2}$ (83.98 eV) photoelectron lines. For self-consistency, the C $1s$ line at 284.6 eV was used as a reference for all charge shift corrections as this peak arises from hydrocarbon contamination and its binding energy is generally accepted as remaining constant, irrespective of the chemical state of the sample. For XPS measurements, a glass rod from each composition was cleaved in the analysis chamber at a base pressure 2×10^{-9} mbar before being transferred to the analysis

chamber where the pressure was maintained at $<2\times10^{-10}$ mbar. Each sample was fractured in this manner to reduce the signal from oxygen and carbon contamination from the atmosphere and, correspondingly, to provide a surface more representative of the bulk. The base pressure in the analysis chamber during these measurements was less than 5×10^{-10} mbar.

The temperature-dependent dc magnetization was measured using a superconducting quantum interference device (SQUID) magnetometer (Quantum Design model MPMS-5S) in a magnetic field of 5000 Oe over a temperature range of 5–300 K at temperature intervals of 2.5 K. The susceptibility of the sample holder is negligible below 100 K for all samples and less than a 2% correction at the highest temperature for all samples. The overall accuracy of the magnetic measurements is estimated to be ~3% due to the uncertainty of the magnetometer calibration.

III. RESULTS

A. XPS spectra of Sr 3*p* and B 1*s*

The core level Sr 3*p* spectra for the three series of glasses as well as for SrO powder are shown in Fig. 1 with the corresponding peak positions and full width at half maxima (FWHM) listed in Table II. The doublet peaks attributed to Sr $3p_{3/2}$ and Sr $3p_{1/2}$ in the Sr 3*p* spectra for all glass samples have essentially the same binding energies and FWHM independent of the composition, but are shifted by about 0.5–0.6 eV, on the average, toward higher binding energies in comparison to their values in SrO powder. This shift to higher binding energies probably arises from a difference in the molecular environment surrounding the Sr atom between the SrO structure and the vanadate or borovanadate glass structures. Although the next-nearest neighbors are all Sr atoms in SrO, they are progressively replaced by V or B atoms in these glass systems. The larger Pauling electronegativities for V (1.63) and B (2.04) than that for Sr (0.95) results in V and B having higher affinities for electrons than Sr. Thus, the electron density at the Sr atomic sites decrease with the addition of V and B and lead to a shift to higher Sr 3*p* binding energies in these glasses. Upon closer inspection of the Sr 3*p* binding energies in Table II, one does indeed note a small discernible decrease in the Sr 3*p* peak position with increasing Sr content in the series I and II glasses, consistent with this discussion.

On the other hand, the binding energies determined from the B 1*s* spectra for the two borovanadate glass systems are shifted to lower energies than that determined from B_2O_3 powder and appear to increase with increasing B content (see Fig. 2 and Table II). The reason for this can also be explained in terms of the local molecular environment and the relative Pauli electronegativities. That is, the dilution of the next-nearest neighbors of B in the B_2O_3 local structure with V and Sr will result in a shift of the B 1*s* binding energy to a lower value and a gradual decrease in the B 1*s* binding energies with decreasing B content, as the V and Sr atoms have smaller electron affinities.

B. XPS spectra of V 2*p* and magnetic susceptibility results

Figure 3 shows the V 2*p* core level spectra for the glass samples as well as the spectra for V_2O_5 powder. The V 2*p*

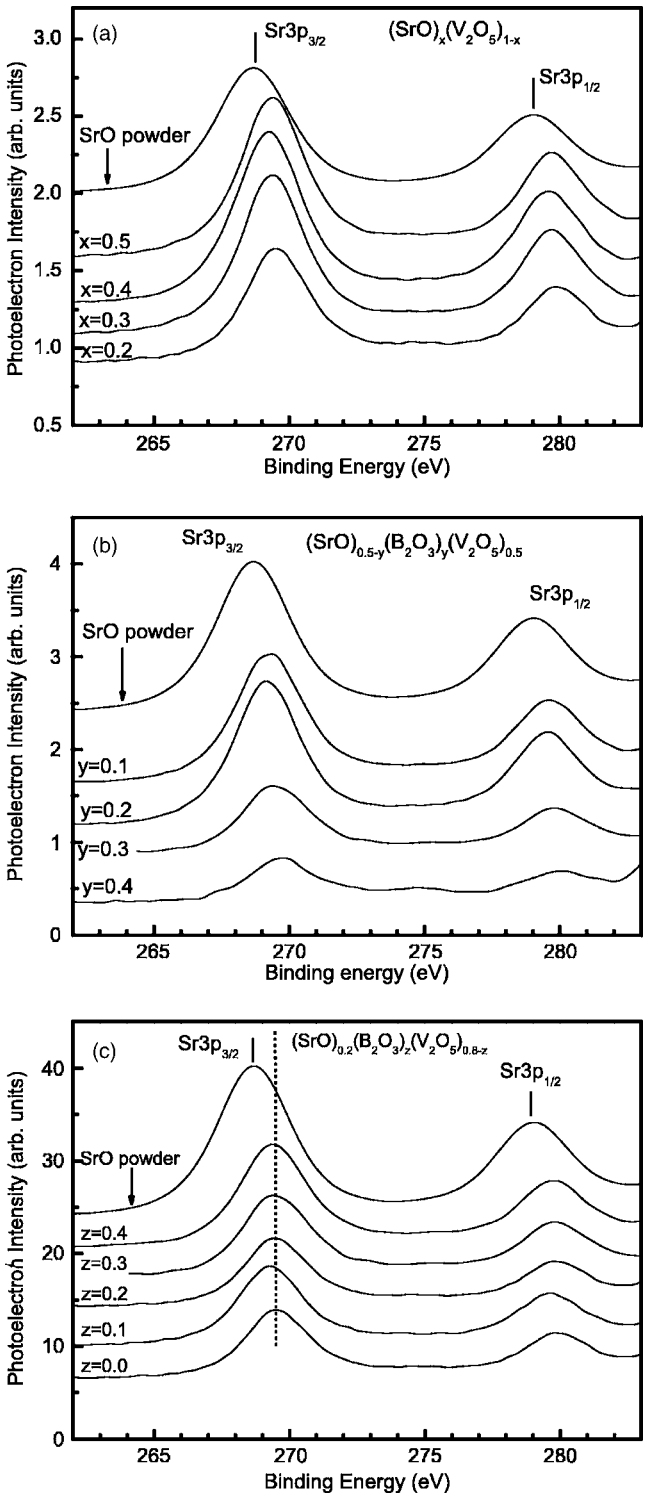

FIG. 1. Sr 3*p* spectra for the (a) $(SrO)_x(V_2O_5)_{1-x}$ [I], (b) $(SrO)_{0.5-y}(B_2O_3)_y(V_2O_5)_{0.5}$ [II], and (c) $(SrO)_{0.2}(B_2O_3)_z(V_2O_5)_{0.8-z}$ [III] glasses and for SrO powder.

spectra exhibit spin-orbit components, V $2p_{3/2}$ and V $2p_{1/2}$, at binding energies of about 517 and 525 eV. The doublet peaks attributed to V $2p_{3/2}$ and V $2p_{1/2}$ in the V 2*p* spectra are essentially at the same energies for all glass samples independent of the composition but shifted by about 0.25 eV, on the average, toward higher binding energies in compari-

TABLE II. Peak positions in electron volts and their corresponding FWHM for the core levels V $2p$, Sr $3p$, B $1s$, and O $1s$ in Sr-vanadate $(SrO)_x(V_2O_5)_{1-x}$ [I] and Sr-borovanadate $(SrO)_{0.5-y}(B_2O_3)_y(V_2O_5)_{0.5}$ [II] and $(SrO)_{0.2}(B_2O_3)_z(V_2O_5)_{0.8-z}$ [III] glasses. The uncertainty is ±0.10 eV in the peak position and ±0.20 eV in FWHM.

Series	x,y,z	V $2p_{3/2}$[a] (FWHM)	V $2p_{1/2}$[a] (FWHM)	ΔV $2p$	Sr $3p_{3/2}$ (FWHM)	Sr $3p_{1/2}$ (FWHM)	ΔSr $3p$	B $1s$ (FWHM)	O $1s$[a] (FWHM)
I	0.2	517.60 (1.91)	525.13 (2.39)	7.53	269.47 (2.76)	279.83 (2.73)	10.36	—	530.59 (1.83)
	0.3	517.52 (1.92)	525.00 (2.33)	7.48	269.30 (2.87)	279.60 (2.69)	10.30	—	530.51 (1.82)
	0.4	517.47 (1.86)	525.00 (2.39)	7.53	269.22 (2.96)	279.45 (2.75)	10.23	—	530.44 (1.98)
	0.5	517.45 (2.02)	524.98 (2.43)	7.53	269.20 (2.53)	279.45 (2.79)	10.25	—	530.38 (2.02)
II	0.0	517.45 (2.02)	524.98 (2.43)	7.53	269.20 (2.53)	279.45 (2.79)	10.25	—	530.38 (2.02)
	0.1	517.56 (1.91)	525.05 (2.37)	7.49	269.22 (2.95)	279.58 (2.76)	10.36	191.95 (1.94)	530.54 (2.16)
	0.2	517.40 (1.92)	524.98 (2.33)	7.58	269.12 (2.87)	279.56 (2.69)	10.44	191.98 (1.97)	530.33 (2.12)
	0.3	517.44 (1.86)	524.97 (2.39)	7.53	269.31 (2.96)	279.78 (2.79)	10.47	192.34 (1.94)	530.42 (2.60)
	0.4	517.48 (2.02)	524.90 (2.43)	7.52	269.55 (2.53)	279.81 (2.79)	10.26	192.57 (1.69)	530.35 (2.20)
III	0.0	517.60 (1.91)	525.13 (2.39)	7.53	269.47 (2.76)	279.83 (2.73)	10.36	—	530.59 (1.83)
	0.1	517.44 (1.84)	525.00 (2.41)	7.56	269.33 (2.70)	279.60 (2.68)	10.27	192.09 (1.91)	530.43 (1.96)
	0.2	517.40 (1.96)	524.92 (2.41)	7.52	269.22 (2.82)	279.57 (2.60)	10.35	192.14 (1.84)	530.43 (2.09)
	0.3	517.44 (1.86)	524.97 (2.39)	7.53	269.31 (2.96)	279.78 (2.79)	10.47	192.34 (1.94)	530.42 (2.60)
	0.4	517.45 (1.83)	525.02 (2.22)	7.57	269.34 (2.95)	279.71 (2.68)	10.37	192.22 (1.89)	530.63 (2.69)
V_2O_5		517.25 (1.76)	524.72 (2.57)	7.47					530.12 (1.85)
SrO					268.69 (3.11)	279.00 (2.99)	10.31		529.02 (2.57)
B_2O_3								192.85 (2.15)	533.05 (2.68)

[a]These peak positions are the average of two peaks.

son to their values in V_2O_5 powder. Upon careful inspection of the V $2p_{3/2}$ spectra, however, an asymmetry is observable on the lower binding energy side of the core level, which is indicative of V existing in more than one oxidation states in these glasses.[37] Furthermore, the appearance of a small satellite peak at about 3 eV on the higher binding energy side of the main V $2p_{3/2}$ peak provides additional evidence for the presence of V^{4+} $(3d^1)$ ions in these glasses as such satellites are observed for certain transition metal and rare earth compounds that have unpaired electrons in $3d$ or $4f$ shells, respectively.[38] Hence, each V $2p_{3/2}$ spectrum was fitted to two Lorentzian-Gaussian peaks with the lower binding energy corresponding to V^{4+} and the higher binding energy peaks to V^{5+}.[39] An example of this fitting procedure is shown in Fig. 4. Using these peak areas, the ratio of V^{4+}/V_{total} was calculated as follows:

$$V^{4+} = (\text{area of peak 1}) = A1,$$

$$V^{5+} = (\text{area of peak 2}) = A2,$$

$$V^{4+}/V_{total} = V^{4+}/(V^{4+} + V^{5+}) = A1/(A1 + A2).$$

The resulting area ratios (see Table III) indicate that more than 90% of V ions are in the V^{5+} state, which is consistent with the magnetic susceptibility results.

The magnetic susceptibility data for the $(SrO)_x(V_2O_5)_{1-x}$ glass series are displayed in Fig. 5 as plots of the inverse magnetic susceptibility, H/M, as a function of the temperature T. The susceptibility data do not appear to follow a simple Curie-Weiss behavior $[M/H = C/(T-\theta)]$ as there is a distinct downward curvature in the data over the entire temperature range. After attempting several other fitting possibilities, it was found that the data for each sample could be fitted to a positive temperature-independent constant plus the Curie-Weiss temperature-dependent term. The temperature-independent constants were determined from a high-temperature extrapolation of M/H versus $1/T$ plots for temperatures above 200 K. After subtracting these temperature-independent constants from the measured susceptibility data, the resulting $M^*/H[=M/H-(M/H)_{constant}]$ data follow a Curie-Weiss behavior as also demonstrated in Fig. 6.

The magnetic susceptibility data for the other two series of glasses, $[(SrO)_{0.5-y}(B_2O_3)_y(V_2O_5)_{0.5}]$ and $[(SrO)_{0.2}(B_2O_3)_z(V_2O_5)_{0.8-z}]$, also show a similar behavior and were fitted to a temperature-independent term plus the temperature-dependent Curie-Weiss contribution following a similar procedure (see Ref. 22). The resulting parameters — $(M/H)_{constant}$, the Curie constant C, and the paramagnetic Curie temperature θ — obtained from this fitting procedure are listed in Table IV for all samples. One notes that the magnitude of the temperature-independent term, $(M/H)_{constant}$, is about an order of magnitude smaller than the Curie-Weiss contribution at room temperature. The temperature-independent contribution can be expected to be present in these oxide glasses as the V^{5+}, Sr^{2+}, B^{3+}, and O^{2-} ions will give rise to a temperature-independent diamagnetic contribution, while V_2O_5 gives a temperature-independent paramagnetic contribution on the order of 10^{-4} emu/mol Oe.[40] Since this latter value is an order of magnitude

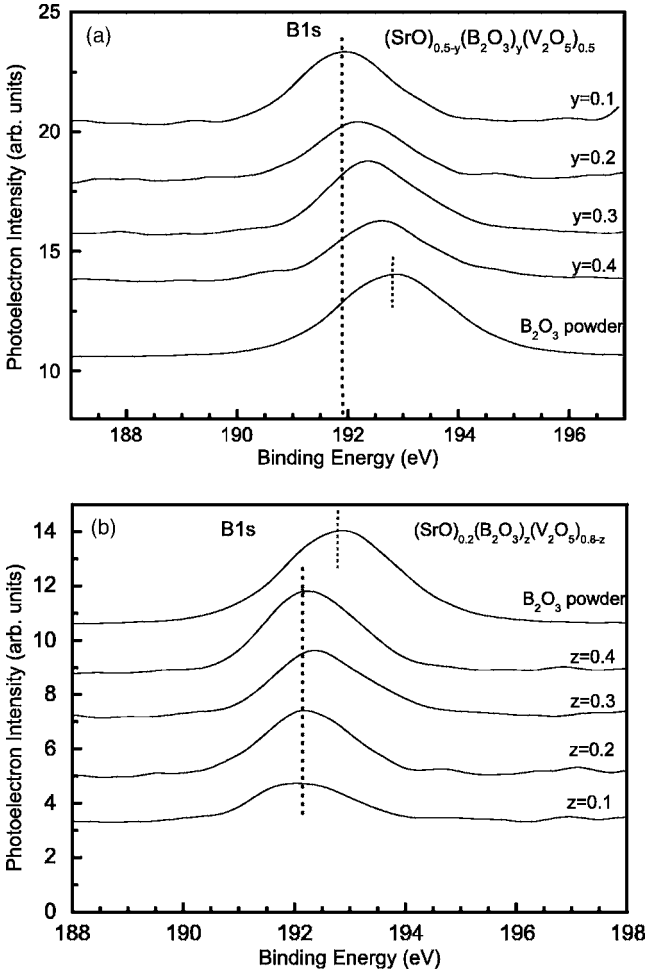

FIG. 2. B 1*s* spectra for the (a) $(SrO)_{0.5-y}(B_2O_3)_y(V_2O_5)_{0.5}$ [II] and (b) $(SrO)_{0.2}(B_2O_3)_z(V_2O_5)_{0.8-z}$ [III] glasses and for B_2O_3 powder.

larger than the typical diamagnetic contributions from the core ions, one can expect that the V_2O_5 paramagnetic contribution will dominate over the response arising from the core diamagnetism of the glass ions. This is in agreement with the experimental evidence of $(M/H)_{\text{constant}}$ being positive. Furthermore, this interpretation is consistent with the V_2O_5 concentration dependence of $(M/H)_{\text{constant}}$ for the entire series of glasses. For example, $(M/H)_{\text{constant}}$ for the $(SrO)_x(V_2O_5)_{1-x}$ glasses increases with an increase in the vanadium content.

Since V^{5+} ions are nonmagnetic, the Curie-Weiss behavior observed in these glasses must be associated with a fraction of the vanadium ions being in another oxidation state, most probably V^{4+} as suggested by the x-ray photoelectron spectroscopy studies performed on these glasses. Thus, the determination of the Curie-Weiss parameters in conjunction with concentration determinations by chemical analysis on these oxide glasses result in magnetic V^{4+} ions ($p_{\text{eff}} = 1.73\ \mu_B$) being present in concentrations between 2 and 10% of the total V concentration for these glasses. These percentages are consistent with other recent results[21] on strontium-vanadate glasses and in reasonably good agreement with the XPS studies performed on these glasses.

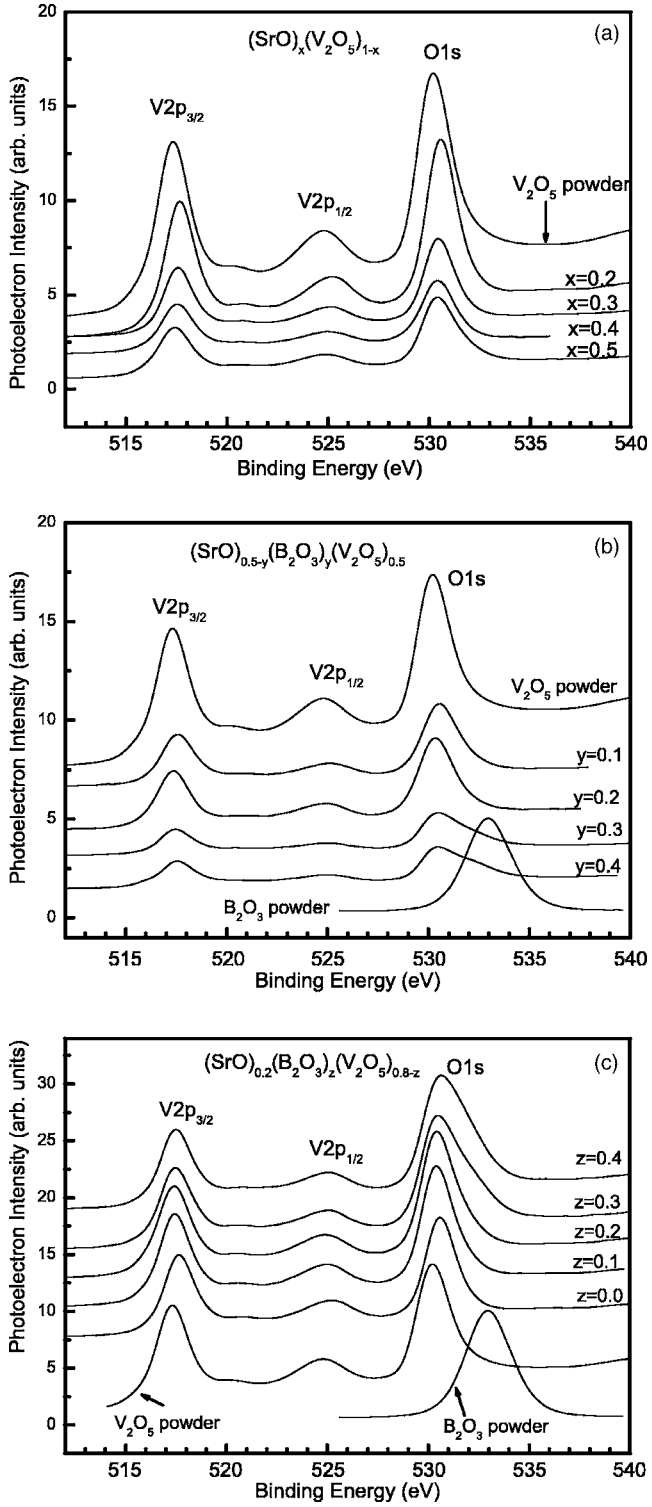

FIG. 3. V 2*p* and O 1*s* spectra for the (a) $(SrO)_x(V_2O_5)_{1-x}$ [I], (b) $(SrO)_{0.5-y}(B_2O_3)_y(V_2O_5)_{0.5}$ [II], and (c) $(SrO)_{0.2}(B_2O_3)_z(V_2O_5)_{0.8-z}$ [III] glasses as well as for V_2O_5 and B_2O_3 powders.

The θ values found in the present measurements of these vanadate glasses are found to range from 0 to -2.8 K, indicating a weak antiferromagnetic interaction between the V^{4+} ions. Typically, the values of θ are proportional to the strength of the interaction and the number of neighboring

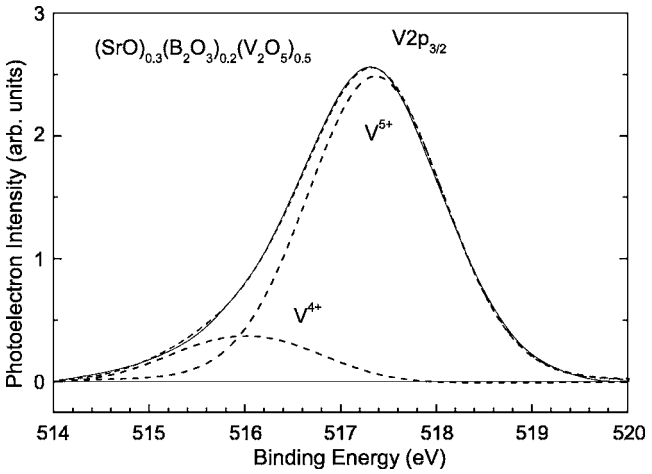

FIG. 4. V $2p_{3/2}$ spectrum (points) for the $(SrO)_{0.3}(B_2O_3)_{0.2}(V_2O_5)_{0.5}$ glass and the resulting peaks from a least-squares fitting routine (dashed lines).

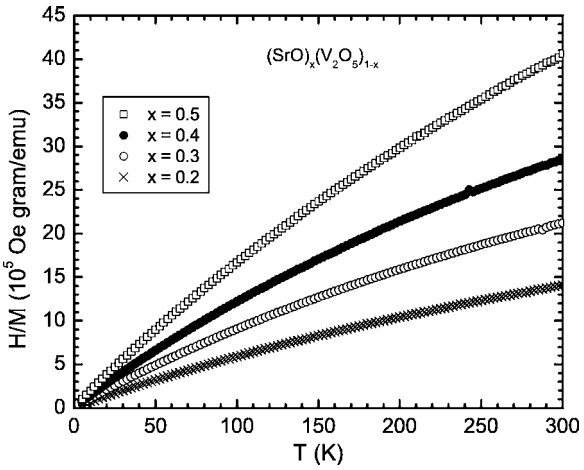

FIG. 5. The inverse of the magnetic susceptibility M/H as a function of temperature for $(SrO)_x(V_2O_5)_{1-x}$ [I] glasses.

magnetic ions. Assuming a glass network structure consisting of mainly VO_5 polyhedra or VO_4 tetrahedra,[21] any interactions between the V^{4+} ions result from superexchange interactions through V—O—V bonds. Owing to the low content of V^{4+} ions in these vanadate glasses, V^{4+} would exist predominantly as isolated species in these concentrated vanadate glasses with a limited number of V^{4+}—O—V^{4+} bonds being present.

C. XPS spectra of O 1*s*

The core level spectra for O 1*s* are also shown in Fig. 3. The O 1*s* peak positions for the three series of glass samples appear to be essentially independent of the glass composition but shifted by ~0.4–0.5 eV toward higher binding energies in comparison to their values in V_2O_5 powder and shifted by ~2.5 eV toward lower binding energies in comparison to their values in B_2O_3. However, on closer inspection, the O 1*s* main peaks for two glass samples of the $(SrO)_x(V_2O_5)_{1-x}$ series (x=0.4 and 0.5) as well as all for all Sr-borovanadate glasses (series II and III) are asymmetric and broader. Both the asymmetry and broadening of the O 1*s* peaks in these glasses suggest the existence of at least two different types of oxygen sites being present. Therefore, all O 1*s* spectra were deconvoluted into two Lorentzian-Gaussian peaks corresponding to O 1*s*(1) and O 1*s*(2) with a linear background by means of a least-squares-fitting program as shown in Fig.

TABLE III. Peak positions, FWHM, normalized peak areas, peak separation, and the ratio $V^{4+}/V_{total} = A1/(A1+A2)$ resulting from the curve fitting of the V $2p_{3/2}$ peaks for Sr-vanadate $(SrO)_x(V_2O_5)_{1-x}$ [I] and Sr-borovanadate $(SrO)_{0.5-y}(B_2O_3)_y(V_2O_5)_{0.5}$ [II] and $(SrO)_{0.2}(B_2O_3)_z(V_2O_5)_{0.8-z}$ [III] glasses. The uncertainty is ±0.10 eV in the peak position, ±0.20 eV in FWHM, and ±3.0 in the normalized peak area.

Series	x,y,z	V $2p_{3/2}$(1) (FWHM) [peak area A_1]	V $2p_{3/2}$(2) (FWHM) [peak area A_2]	Δ V $2p_{3/2}$	V^{4+}/V_{total} $[=A_1/(A_1+A_2)]$
I	x=0.2	516.60 (1.72) [6.07]	517.62 (1.72) [93.93]	1.02	0.061
	x=0.3	516.50 (1.69) [3.32]	517.54 (1.69) [96.68]	1.04	0.033
	x=0.4	516.45 (1.69) [7.54]	517.50 (1.82) [92.46]	1.05	0.075
	x=0.5	516.40 (1.78) [4.63]	517.45 (1.83) [95.37]	1.05	0.046
II	y=0.0	516.40 (1.78) [4.63]	517.45 (1.83) [95.37]	1.05	0.046
	y=0.1	516.52 (1.77) [8.78]	517.62 (1.82) [91.22]	1.10	0.088
	y=0.2		517.34 (1.90) [100.00]		0.000
	y=0.3	516.43 (1.74) [7.02]	517.46 (1.79) [92.98]	1.03	0.070
	y=0.4	516.42 (1.84) [7.43]	517.45 (1.83) [95.37]	1.03	0.074
III	z=0.0	516.60 (1.72) [6.07]	517.62 (1.72) [93.93]	1.02	0.061
	z=0.1	516.42 (1.70) [8.54]	517.44 (1.75) [91.46]	1.02	0.085
	z=0.2	516.35 (1.75) [12.46]	517.39 (1.85) [87.54]	1.04	0.125
	z=0.3	516.43 (1.74) [7.02]	517.46 (1.79) [92.98]	1.03	0.070
	z=0.4	516.43 (1.73) [4.37]	517.45 (1.78) [95.63]	1.02	0.044

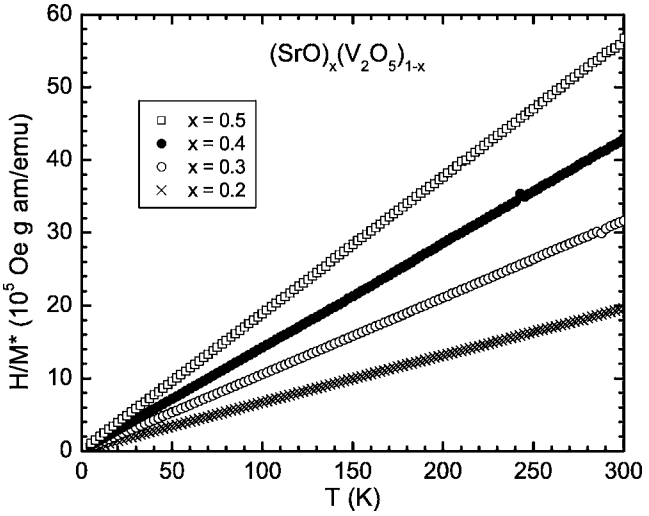

FIG. 6. The inverse of the "corrected" magnetic susceptibility $M^*/H(=M/H-(M/H)_{\text{constant}})$ as a function of temperature for $(SrO)_x(V_2O_5)_{1-x}$ [I] glasses.

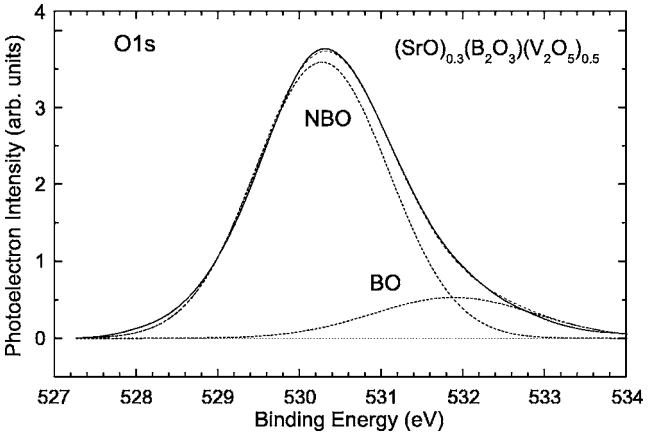

FIG. 7. O 1*s* spectrum for the $(SrO)_{0.3}(B_2O_3)_{0.2}(V_2O_5)_{0.5}$ glass and the resulting O 1*s*(1) and O 1*s*(2) peaks (dashed lines) from a least-squares fitting routine.

7. Table V summarizes the peak positions of O 1*s*(1) and O 1*s*(1), their FWHM, and the normalized area under each peak.

In most XPS studies of oxide glasses, the O 1*s* spectra are more informative with respect to the structure of the glass than the cation spectra.[32–36] Specifically, the binding energy of the O 1*s* electrons is a measure of the extent to which electrons are localized on the oxygen or in the internuclear region, a direct consequence of the nature of the bonding between the oxygen and different cations. If the O 1*s* peaks for the glasses are composed of more than one component peak, then each peak may correspond to the oxygen atoms in some of the following structural units: B—O—B, B—O—V, V—O—V, B—O—Sr, V—O—Sr, V═O, etc., and the area under the peak reflects the relative abundance of these structural units. Clearly, the O 1*s* core-level spectra of Figs. 3 and 7 and Table V indicate that the peak position, FWHM, O 1*s* separation (ΔO 1*s*), and integrated peak area show significant composition-dependent changes. The interpretation of the structures based on these XPS spectra and other studies is described in more detail in Secs. III D and III E.

D. Structure of Sr-vanadate glasses

Previous IR-spectra studies of Dimitriev *et al.*[11] demonstrated that a very intense absorption band at 1020 cm^{-1} arises from the isolated V═O bond in the VO_5 trigonal bipyramid structure in crystalline V_2O_5, where each V ion is fivefold coordinated. The addition of an alkaline earth

TABLE IV. Magnetic susceptibility characterization parameters for Sr-vanadate $(SrO)_x(V_2O_5)_{1-x}$ [I] and Sr-borovanadate $(SrO)_{0.5-y}(B_2O_3)_y(V_2O_5)_{0.5}$ [II] and $(SrO)_{0.2}(B_2O_3)_z(V_2O_5)_{0.8-z}$ [III] glasses.

Series	x,y,z	$(M/H)_{\text{const}}$ (10^{-7} emu/g Oe)	C (10^{-4} emu K/g Oe)	θ (K)	V^4+/V_{total}
I	x=0.2	2.00	1.54	−2.85	0.0427
	x=0.3	1.55	0.955	−0.05	0.0289
	x=0.4	1.17	0.700	0.03	0.0236
	x=0.5	0.700	0.533	−0.91	0.0206
II	y=0.0	0.700	0.533	−0.91	0.0206
	y=0.1	0.670	0.603	−0.07	0.0225
	y=0.2	0.630	0.731	0.42	0.0270
	y=0.3	2.00	0.771	−5.65	0.0276
	y=0.4	1.76	0.617	−7.41	0.0204
III	z=0.0	2.00	1.54	−2.85	0.0427
	z=0.1	1.67	2.47	−1.94	0.0721
	z=0.2	2.00	3.24	−2.64	0.1007
	z=0.3	2.00	0.771	−5.65	0.0276
	z=0.4	0.950	0.734	−1.88	0.0283

TABLE V. Peak positions, FWHM, normalized peak areas, peak separation, and calculated ratio of NBO/TO for Sr-vanadate $(SrO)_x(V_2O_5)_{1-x}$ [I] and Sr-borovanadate $(SrO)_{0.5-y}(B_2O_3)_y(V_2O_5)_{0.5}$ [II] and $(SrO)_{0.2}(B_2O_3)_z(V_2O_5)_{0.8-z}$ [III] glasses. The uncertainty is ±0.10 eV in the peak position, ±0.20 eV in FWHM, and ±3.0 in the normalized peak areas.

Series	x,y,z	O 1s(1) (FWHM) [peak area]	O 1s(2) (FWHM) [peak area]	ΔO 1s	NBO/TO [Eq. (1) or (3)]
I	$x=0.2$	530.52 (1.69) [85.1]	531.60 (1.90) [14.9]	1.08	0.860
	$x=0.3$	530.42 (1.72) [84.4]	531.36 (1.92) [15.6]	0.96	0.898
	$x=0.4$	530.43 (1.98) [100.0]			0.946
	$x=0.5$	530.39 (2.03) [100.0]			1.000
II	$y=0.0$	530.39 (2.03) [100.0]			1.000
	$y=0.1$	530.50 (1.90) [81.0]	531.66 (2.10) [19.0]	1.16	0.891
	$y=0.2$	530.25 (1.85) [79.3]	531.50 (2.30) [20.8]	1.25	0.751
	$y=0.3$	530.39 (1.79) [61.2]	532.00 (2.30) [38.8]	1.61	0.649
	$y=0.4$	530.38 (1.70) [53.6]	532.04 (2.44) [46.2]	1.66	0.619
III	$z=0.0$	530.52 (1.69) [85.1]	531.60 (1.90) [14.9]	1.08	0.860
	$z=0.1$	530.33 (1.66) [77.1]	531.50 (1.96) [22.9]	1.17	0.808
	$z=0.2$	530.34 (1.70) [73.1]	531.63 (2.04) [26.9]	1.29	0.754
	$z=0.3$	530.39 (1.79) [61.2]	532.00 (2.30) [38.8]	1.61	0.649
	$z=0.4$	530.48 (1.85) [57.2]	531.93 (2.42) [42.8]	1.45	0.635

(20 mol % MO=SrO,CaO,BaO) results in a decrease in the intensity of the 1020 cm^{-1} band and the appearance of another band in the vicinity of 970 cm^{-1}. This 1020 cm^{-1} band vanishes completely for 40 mol % alkaline-earth glass samples, while the 970 cm^{-1} band remains. Since only a single crystal phase MV_2O_6 is known to form up to 50 mol % MO, the authors hypothesize that VO_4 groups are immediately formed in the glass and associate into chains upon the introduction of MO. The vibrations associated with the resulting free VO_2 groups in these VO_4 polyhedra would correspondingly shift the frequency of the V=O band from 1020 cm^{-1} to 970 cm^{-1}. With increasing SrO content (40–50 mol %), the structural polyhedron VO_4 then forms metavanadate chains and the VO_5 groups are completely destroyed. Moreover, these authors contend that these spectral results are consistent with a structural model having M^{2+} ions occupying interstitial sites distributed among the chains, whereas M^{2+} ions occupying substitutional sites should have less of an effect on the vibrational frequency shift of the V=O bond of the VO_5 polyhedra with the addition of MO and the subsequent formation of the VO_4 polyhedra.

On the other hand, the IR studies by Sen and Ghosh[21] find only the 1020 cm^{-1} band for the 10 and 20 mol % SrO vanadate glasses and a shift of the band from 970 to 910 cm^{-1} for the 30–50 mol % SrO glasses. Based on these observations, these authors contend that the low SrO content glasses would remain in a VO_5 polyhedral chain with the Sr ions in substitutional sites and that the absorption band shift for the higher SrO content glasses results from the Sr occupying interstitial sites that directly affect the vibrational frequency of the V=O bond. Moreover, the glass structure for these higher Sr-containing glasses would consist of VO_4 polyhedra. However, the interpretation of Sr initially going into the VO_5 structure substitutionally appears to be also inconsistent with earlier studies on the alkaline and alkaline-earth metavanadates, which indicate that the alkaline-earth ions are situated between the chains. Instead of invoking a substitutional model for the apparent different experimental observations at low Sr content, the appearance of the 1020 cm^{-1} and 970 cm^{-1} bands for 20 mol % SrO vanadate glasses may be a just a question of the relative intensity of these bands around this SrO concentration. It is reasonable to assume that the intensity of the 970 cm^{-1} band grows owing to the appearance of VO_4 tetrahedra associated with the SrV_2O_6 formation as more SrO is introduced while the intensity of 1020 cm^{-1} band decreases as the VO_5 polyhedra are destroyed. Between about 10 and 30 mol % SrO, the 970 cm^{-1} band would be finally observable in the IR spectra and the 1020 cm^{-1} band would vanish with the order of appearance and disappearance of these bands predicated on the local concentration variation, instrumental sensitivity, and so forth. Thus, both experimental observations can be successfully interpreted with the Sr occupying interstitial sites between the metavanadate chains.

Based on the above IR results and structural model, it would be reasonable to hypothesize that the Sr-vanadate glasses, $(SrO)_x(V_2O_5)_{1-x}$, studied in this investigation with 20 mol % SrO and greater would consist of a mixture of VO_5 groups (probably trigonal bipyramids) and VO_4 metavanadate chains with the Sr^{2+} ions occupying interstitial sites among the chains. This conjecture is further supported by a very recent study on the structure of alkaline-earth vanadate glasses by Hoppe *et al.*[25] This study not only indicates that the three-dimensional glass network formed by VO_5 and VO_4 units transform to chains of VO_4 units with increasing alkaline-earth content where the VO_n are mainly linked by corners, but that the alkaline-earth oxygen coordination num-

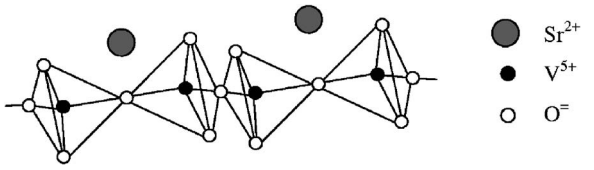

FIG. 8. Metavanadate chain-like structure of SrV_2O_6.

ber is at least six. It is difficult to envision a vanadate structure with the alkaline earth being in a substitutional site and still having a coordination number of 6.

If the glass structure for SrV_2O_6 is comprised of metavanadate chains (see Fig. 8) as in the crystalline material, then this would result in two bridging oxygen (BO) or V—O—V bonds per formula unit of SrV_2O_6 (one BO per each VO_4 metavanadate unit), or a BO/TO ratio of $\frac{1}{3}$, where TO refers to the total number of oxygen atoms per formula unit. Likewise, the V_2O_5 crystalline structure has only one NBO (nonbridging oxygen) due to the single V=O bond in each VO_5 polyhedron and thus a BO/TO ratio of $\frac{3}{5}$. Clearly, a simple mixture of SrV_2O_6 and V_2O_5 crystallinelike structures would overestimate the BO/TO ratios assuming that the BO binding energies for both structures are the same. One would expect a smaller number of bridging oxygen BO per VO_n polyhedron in the glassy network since the crystalline structure is not maintained and fewer corner oxygens will be bridging with other VO_n polyhedra. Conversely, more oxygen sites in the glass network should be classified as nonbridging oxygen NBO than that given by a simple mixture of SrV_2O_6 (NBO/TO=2/3) and V_2O_5 (NBO/TO=2/5) crystallinelike structures. Assuming the area under the lower binding-energy O 1*s* peak [labeled as O 1*s*(1)] for our Sr-vanadate glasses is representative of the relative number of NBO, then the experimentally determined area ratios under O 1*s*(1) ranging from 0.85 to 1.0 are significantly larger than this simple mixture model predicts. Thus the V^{5+} ions would have to form isolated orthovanadate structures (4 NBO and zero BO per VO_4 tetrahedron) and pyrovanadate structures (3 NBO and 1 BO per VO_4 tetrahedron) in addition to metavanadate structures (2 NBO and 2 BO per VO_4 tetrahedron) and VO_5 polyhedral structures (single NBO and 4 BO). In order to maintain charge neutrality, an appropriate number of interstitial Sr^{2+} ions need to be in close proximity to the various structures.

Surprisingly, remarkably good agreement (see Table V) is found with the experimentally normalized peak areas under the lower binding energy O 1*s* peak for the Sr-vanadate glass series as well as for our earlier results on the PbO-vanadate glass series to the following simple formula:

$$\mathrm{NBO/TO} = (2[\mathrm{SrO}] + 4[\mathrm{V_2O_5}])/([\mathrm{SrO}] + 5[\mathrm{V_2O_5}]), \quad (1)$$

where [SrO] represents the relative SrO concentration; $[V_2O_5]$ (=1−[SrO]), the V_2O_5 concentration; and TO, the total number of oxygen. Alternatively, the BO/TO ratio [normalized area under the higher binding energy O 1*s* peak labeled as O 1*s*(2)] would be given as

$$\begin{aligned}\mathrm{BO/TO} &= 1 - \mathrm{NBO/TO} \\ &= (1 - 2[\mathrm{SrO}])/(5 - 4[\mathrm{SrO}]) \\ &= ([\mathrm{V_2O_5}] - [\mathrm{SrO}])/([\mathrm{SrO}] + 5[\mathrm{V_2O_5}]). \quad (2)\end{aligned}$$

Equation (2) provides further insight into the local glass network structure as there would be one bridging oxygen for each V_2O_5 unit, or more correctly, one oxygen whose local environment in the VO_5 polyhedral structure results in a higher binding energy. With the addition of SrO, a V_2O_5 unit would then transform into SrV_2O_6 with no bridging oxygen, that is, no oxygen having similar binding energies or local environments as the single bridging oxygen in VO_5 polyhedra. Moreover, this simple vanadate glass model consisting of V_2O_5 units with one bridging oxygen (probably due to the highly distorted VO_5 polyhedral structures) and SrV_2O_6 units with no bridging oxygen would also be consistent with the interpretation based on the IR spectra studies[11] on alkaline-earth vanadate glasses. Thus, Eqs. (1) and (2) could be rewritten in terms of the structural units as

$$\mathrm{NBO/TO} = (6[\mathrm{SrV_2O_6}] + 4\{[\mathrm{V_2O_5}] - [\mathrm{SrV_2O_6}]\})/([\mathrm{SrO}] + 5[\mathrm{V_2O_5}]),$$

and

$$\mathrm{BO/TO} = ([\mathrm{V_2O_5}] - [\mathrm{SrV_2O_6}])/([\mathrm{SrO}] + 5[\mathrm{V_2O_5}]),$$

where $[SrV_2O_6]$ represents the concentration of SrV_2O_6 (=[SrO]) and $\{[V_2O_5]-[SrV_2O_6]\}$, the concentration of V_2O_5 remaining in the VO_5 polyhedral structure with one bridging oxygen, or equivalently the concentration of oxygen sites in a particular V—O—V bond that has a higher binding energy than all other oxygen sites.

E. Structure of Sr-borovanadate glasses

Structure investigations of borovanadate glasses are less numerous than those for the vanadate glasses. Recently, Raman and EXAFS spectroscopic techniques[27,28] have been used to determine the structure of borovanadate glasses with ZnO and Li_2O dopants. The ZnO-borovanadate glasses, which are probably more similar to our SrO-borovanadate glass series, found VO_4 to be the predominated polyhedra with the symmetry around the V^{5+} ions being more distorted in comparison to the crystalline materials. With increasing V_2O_5 content relative to B_2O_3, the distorted VO_4 tetrahedra would initially be incorporated into the borate groupings of the BO_3 and BO_4 units. At higher concentrations, these metavanadate groups could be connected to each other directly forming possibly metavanadate chain structures. Moreover, the Stevels' structural parameter decreases with the incorporation of VO_4 and thus indicates a reduction in the average number of bridging oxygen per network-forming polyhedron.[27] Another structural study of the strontium borate glass system[41] indicates that the Sr ions act only as a network modifier with a coordination number of 6 as determined from the EXAFS measurements. Based on these studies, we speculate that the local structure of the Sr-borovanadate glasses is quite similar to the Sr-vanadate glasses except that BO_3 polyhedra are substituted for the

VO_n polyhedral units. This substitution of BO_3 polyhedra into the VO_5 glass structure is also in accordance with the Dimitriev's interpretation of the IR spectra on a 20 mol % B_2O_3 vanadate glass[11] that only exhibited a vibration band at 1020 cm^{-1}. However, the question remains as to whether the oxygens surrounding the boron ions have binding energies or environments similar to that of the higher binding energy bridging oxygen in the VO_5 polyhedra or are more representative of the lower binding energy nonbridging oxygen.

Similar to the Sr-vanadate glass series, the experimentally normalized peak areas under the lower binding energy O $1s(1)$ peak for the entire Sr-borovanadate glass series are found to be in reasonably good agreement (see Table V) with a formula where NBO depends only on the SrO and V_2O_5 content

$$\mathrm{NBO/TO} = (2[\mathrm{SrO}] + 4[\mathrm{V_2O_5}])/([\mathrm{SrO}] + 3[\mathrm{B_2O_3}] + 5[\mathrm{V_2O_5}]), \quad (3)$$

where the square brackets represents the relative SrO, B_2O_3, and V_2O_5 concentration. Alternatively, the BO/TO ratio would be given by

$$\mathrm{BO/TO} = 1 - \mathrm{NBO/TO} = ([\mathrm{V_2O_5}] - [\mathrm{SrO}] + 3[\mathrm{B_2O_3}])/([\mathrm{SrO}] + 3[\mathrm{B_2O_3}] + 5[\mathrm{V_2O_5}]). \quad (4)$$

A simple structural interpretation of these formulas would be that each V_2O_5 unit has a single bridging oxygen and each B_2O_3 unit would contribute three bridging oxygen. With the incorporation of SrO, a V_2O_5 unit would be transformed into SrV_2O_6 with no bridging oxygen similar to the conjecture for the Sr-vanadate glass series. Since the V_2O_5 content is always greater than the SrO content, the formation of $Sr_2B_2O_5$ would not need to occur. Thus,

$$\mathrm{NBO/TO} = (6[\mathrm{SrV_2O_6}] + 4\{[\mathrm{V_2O_5}] - [\mathrm{SrV_2O_6}]\})/([\mathrm{SrO}] + 3[\mathrm{B_2O_3}] + 5[\mathrm{V_2O_5}]),$$

and

$$\mathrm{BO/TO} = (\{[\mathrm{V_2O_5}] - [\mathrm{SrV_2O_6}]\} + 3[\mathrm{B_2O_3}])/([\mathrm{SrO}] + 3[\mathrm{B_2O_3}] + 5[\mathrm{V_2O_5}]),$$

where $[SrV_2O_6]$ again represents the concentration of SrV_2O_6 (=[SrO]) and $\{[V_2O_5]-[SrV_2O_6]\}$, the concentration of V_2O_5 remaining in the VO_5 polyhedral structure with one bridging oxygen.

In order to see if the assignment of the oxygen associated with the boron ions as bridging oxygen is experimentally justifiable, one should look at the O $1s$ spectra analysis as well as the spectra of the cations more critically: (i) in fact, one notes that the position of the O $1s(2)$ peak, which we identify as the bridging oxygen peak, shifts to higher energies by ~0.4 eV and its FWHM becomes broader when the B_2O_3 content exceeds the SrO content for both Sr-borovanadate glasses series II and III, as seen in Table V. This indicates the appearance of a second type of bridging oxygen in the XPS spectra with very similar binding energies to the bridging oxygen V—O—V bond in the VO_5 polyhedral structure. For example, oxygen sites in both V—O—B and B—O—B arising from the substitution of BO_n structures into the vanadate glass network would have higher binding energies compared to oxygen in V—O—V due to the larger electronegativity of B (2.04) as compared to V (1.63). With increasing B_2O_3 concentration, there would be a growing number of oxygen in these V—O—B and B—O—B bonds, which would give rise to a broader O $1s(2)$ peak and even a shift in its peak position. (ii) Although one does find that the V $2p_{3/2}$ and V $2p_{1/2}$ peak positions have a small, but systematic shift ($\leq$0.15 eV) toward lower energies for increasing SrO content for the Sr-vanadate glass series (I) as shown in Table II, both of the V $2p$ peaks are essentially unchanged across the two Sr-borovanadate glass series (II-fixed V_2O_5 and III-fixed SrO). This suggests that the difference in the binding energies between V sites in VO_5 and VO_4 (or SrV_2O_6) polyhedral structures is less than the resolution of our XPS measurements. (iii) On the other hand, the Sr $3p_{3/2}$ and Sr $3p_{1/2}$ peak positions shift toward slightly higher energies with increasing V or B content for glass series I and II. Even for the fixed SrO content glasses of series III, the Sr $2p_{1/2}$ peak position shifts to higher energies with increasing B content and decreasing V content. These shifts to higher energies are consistent with a decreasing electron density at the cation site when the electronegativities of the three cations are taken into account. (iv) Likewise, the B $1s$ peak shifts to lower energies with increasing V_2O_5 or SrO content for both Sr-borovanadate glass series II and III, which is consistent with an increasing electron density at the B site as B has the greatest electron affinity. Thus the qualitative behavior of the various spectra as a function of the composition seems to be consistent with the simple structural model being suggested by Eq. (3).

Although the quantitative agreement is reasonably good over the entire vanadate glass series, the experimental results for the normalized area under the O $1s(1)$ peak exhibit a more rapid change at certain concentrations in all three glass series than the continuous change resulting from the NBO/TO ratio calculated from Eq. (3) [and Eq. (1) when B_2O_3 content is zero]. For example, the normalized O $1s(1)$ peak areas for the Sr-vanadate glasses display a fairly sudden decrease from 100% to ~85% when the Sr concentration drops from 40 to 30 mol %. Likewise, the normalized O $1s(1)$ peak areas drop from the range of 80–73% to <61% when the B_2O_3 content exceeds the SrO content for both Sr-borovanadate glasses series II and III. When combined with the observation that position of the O $1s(2)$ peaks also significantly shifts when the B_2O_3 content exceeds the SrO content, three distinct groupings are evident as seen more clearly in Table VI. Thus, the three regions can be characterized in terms of the following structural units. Group A would be characterized by essentially metavanadate chainlike structures or groups of SrV_2O_6 and individual VO_4 units in which all oxygen sites have similar binding energies of ~530.4 eV and are designated as being of the O $1s(1)$ type. Group B then would be characterized by the appearance of VO_5 polyhedra [observation of an O $1s(2)$ peak in the O $1s$ spectra] in addition to the metavanadate chainlike structures of SrV_2O_6 and fewer VO_4 units. With the introduction of

TABLE VI. Grouping of various Sr-vanadate [I] and Sr-borovanadate [II and III] glasses based on normalized area under O 1*s*(1) peak and the position and FWHM of the O 1*s*(2) peak.

Group	V_2O_5	SrO	B_2O_3	O 1*s*(1) peak area	O 1*s*(2) peak position (FWHM)
A	0.488	0.511		1.000	
	0.591	0.409		1.000	
B	0.692	0.308		0.844	531.36 (1.92)
	0.792	0.208		0.851	531.60 (1.90)
	0.498	0.415	0.087	0.810	531.60 (2.10)
	0.483	0.299	0.218	0.792	531.50 (2.30)
	0.701	0.209	0.091	0.771	531.50 (1.96)
	0.613	0.209	0.178	0.731	531.63 (2.04)
C	0.486	0.192	0.322	0.612	532.00 (2.30)
	0.434	0.220	0.346	0.572	531.93 (2.42)
	0.539	0.112	0.347	0.536	532.04 (2.44)

B_2O_3 into the glass, the B atoms would substitute into the V sites of the various VO_n polyhedra and not radically change the relative weight or position of the two O 1*s* peaks. Upon the B_2O_3 concentration exceeding the SrO content, group C is realized as the O 1*s*(2) peak shifts and broadens, indicating another possible type of oxygen binding site. Since the appearance of the O 1*s*(2) peak shift is accompanied by both the B 1*s* and Sr 3*p* peak positions shifting to higher energies, one can speculate that the BO_n structures may form boronrich regions in the vanadate glass network, such as metaborate chain structures, BO_4 polyhedra, or even $Sr_2B_2O_5$ units. Thus this qualitative picture of three distinct structural groupings for the Sr-vanadate and Sr-borovanadate glasses is remarkably similar to the interpretation of the glass structure based on the previous IR and EXAFS studies on these glasses. To gain further insight into the validity of this structural model, increased resolution over the present XPS capabilities combined with neutron-scattering experiments would be necessary to distinguish between these various structures.

IV. CONCLUSION

The XPS spectra for Sr 3*p*, V 2*p*, O 1*s*, and B 1*s* core levels of SrO-vanadate and SrO-borovanadate glasses have been investigated in order to understand their structural properties. The shifts in the Sr 3*p* and V 2*p* peaks toward higher binding energies in these glasses from their values in SrO and V_2O_5 are understood in terms of the relative electron affinities of Sr, V, and B ions and the change in the next-nearest-neighbor environment with varying cation concentrations. Similar reasoning explains the shift in the B 1*s* peak toward lower energies from that of B_2O_3. The O 1*s* spectra were found to be comprised of two different peaks whose width and area under the peaks varied with the chemical composition. From the analysis of these peaks, three distinct concentration regimes were identified in terms of the structural units being present. The first grouping consisted of the low SrO-containing vanadate glasses and was characterized by metavanadate chainlike structures of SrV_2O_6 and individual VO_4 units, in which all oxygen sites have similar binding energies. The second grouping consisted of higher SrO-containing vanadate glasses and was characterized by the appearance of VO_5 polyhedra in addition to the metavanadate chainlike structures of SrV_2O_6 with fewer VO_4 units. With the introduction of B_2O_3 into these glasses, the B atoms would substitute into the V sites of the various VO_n polyhedra and not result in any additional structural units. Upon the B_2O_3 concentration exceeding the SrO content, a third grouping is realized as BO_n structures, such as metaborate chain structures, BO_4 polyhedra, or $Sr_2B_2O_5$ units, are formed in boronrich regions in the borovanadate glass network in addition to the VO_n polyhedra and SrV_2O_6 structures. Thus this qualitative picture of the local glass structure evolving as the relative concentration varies in these SrO-vanadate and SrO-borovanadate glasses is very similar to the interpretation of the glass structure based on the previous IR and EXAFS studies on these glasses.

ACKNOWLEDGMENTS

The support of the KFUPM Physics Department and Research Committee (Grant No. FT/2002-05) is greatly acknowledged.

[1] A. Ghosh, J. Appl. Phys. **64**, 2652 (1988).
[2] A. Ghosh, Phys. Rev. B **42**, 5665 (1990).
[3] J. Livage, J. P. Jollivet, and E. Tronc, J. Non-Cryst. Solids **121**, 35 (1990).
[4] N. Ichinose and Y. Nakai, J. Non-Cryst. Solids **203**, 353 (1996).
[5] N. F. Mott, J. Non-Cryst. Solids **1**, 1 (1968).
[6] G. Austine and N. F. Mott, Adv. Phys. **18**, 41 (1969).
[7] V. K. Dhawan, A. Mansingh, and M. Sayer, J. Non-Cryst. Solids **51**, 87 (1982).
[8] A. Ghosh and B. K. Chaudhuri, J. Non-Cryst. Solids **83**, 151 (1986).
[9] H. Hirashima and T. Yoshida, J. Non-Cryst. Solids **95-96**, 817 (1987).
[10] H. Mori, T. Kitami, and H. Sakata, J. Ceram. Soc. Jpn. **101**, 347 (1993).
[11] Y. Dimitriev, V. Dimitrov, M. Arnaudov, and D. Topalov, J. Non-Cryst. Solids **57**, 147 (1983).
[12] D. Ilieva, V. Dimitrov, Y. Dimitriev, and G. Bogachev, Phys. Chem. Glasses **40**, 6 (1999).
[13] A. C. Wright, Philos. Mag. B **50**, 23 (1984).
[14] A. C. Wright, C. A. Yarker, P. A. V. Johnson, and R. N. Sinclair, J. Non-Cryst. Solids **76**, 333 (1985).
[15] S. Hayakawa, T. Yoko, and S. Sakka, J. Ceram. Soc. Jpn. **102**, 522 (1994).
[16] S. Hayakawa, T. Yoko, and S. Sakka, J. Ceram. Soc. Jpn. **102**, 530 (1994).
[17] S. Hayakawa, T. Yoko, and S. Sakka, J. Non-Cryst. Solids **183**, 73 (1995).
[18] S. Mandal and A. Ghosh, Phys. Rev. B **48**, 9388 (1993).
[19] S. Sen and A. Ghosh, J. Phys.: Condens. Matter **11**, 1529 (1999).
[20] S. Sen and A. Ghosh, J. Non-Cryst. Solids **258**, 29 (1999).
[21] S. Sen and A. Ghosh, J. Mater. Res. **15**, 995 (2000).
[22] M. Chinkhota, P. S. Fodor, G. D. Khattak, and L. E. Wenger, J. Appl. Phys. **91**, 829 (2002).
[23] G. D. Khattak, N. Tabet, and M. A. Salim, J. Electron Spectrosc. Relat. Phenom. **133**, 103 (2003).
[24] A. Mekki, G. D. Khattak, and L. E. Wenger, J. Non-Cryst. Solids **330**, 156 (2003).
[25] U. Hoppe, R. Kranold, J. M. Lewis, C. P. O'Brien, H. Feller, S. Feller, M. Affatigato, J. Neuefeind, and A. C. Hannon, Phys. Chem. Glasses **44**, 272 (2003).
[26] T. Hübert, G. Mosel, and M. Nofz, Phys. Chem. Glasses **41**, 300 (2000).
[27] T. Hübert, G. Mosel, and K. Witke, Glass Phys. Chem. **27**, 114 (2001).
[28] O. Attos, M. Massot, M. Balkanski, E. Haro-Poniatowski, and M. Asomoza, J. Non-Cryst. Solids **210**, 163 (1997).
[29] H. El Mkami, B. Deroide, N. Abidi, P. Rumori, and J. V. Zanchetta, Phys. Chem. Glasses **38**, 137 (1997).
[30] M. Nabavi, C. Sanchez, and J. Livage, Philos. Mag. B **63**, 941 (1991).
[31] J. Mendialdua, R. Casanova, and Y. Barbaux, J. Electron Spectrosc. Relat. Phenom. **71**, 249 (1995).
[32] R. K. Brow, in *Characterization of Ceramics*, edited by R. E. Loehman (Butterworth-Heinemann, London, 1993).
[33] R. K. Brow, C. M. Arens, X. Yu, and E. Day, Phys. Chem. Glasses **35**, 132 (1994).
[34] B. M. J. Smets and D. M. Krol, Phys. Chem. Glasses **25**, 113 (1984).
[35] G. D. Khattak, M. A. Salim, L. E. Wenger, and A. H. Gilani, J. Non-Cryst. Solids **262**, 66 (2000).
[36] G. D. Khattak, E. E. Khawaja, L. E. Wenger, D. J. Thompson, M. A. Salim, A. B. Hallak, and M. A. Daous, J. Non-Cryst. Solids **194**, 1 (1996).
[37] C. R. Bamford, in *Color Generation and Control in Glass* (Elsevier, Amsterdam, 1977).
[38] D. Briggs and M. P. Seah, in *Practical Surface Analysis*, 2nd ed. (Wiley, New York, 1990), Vol. 1, p. 131.
[39] A. Proctor and P. M. A. Sherwood, Anal. Chem. **52**, 2315 (1980).
[40] Y. Kawamota, J. Tanida, H. Hamada, and H. Kiriyama, J. Non-Cryst. Solids **38-39**, 301 (1980).
[41] T. Hübert, U. Harder, G. Mosel, and K. Witke, in *Borate Glasses, Crystals, and Melts II*, edited by A. C. Wright, S. A. Feller, and A. C. Hannon (Society of Glass Technology, Sheffield, 1997), p. 156.